Mechanism and Machine Theory 196 (2024) 105631

Contents lists available at ScienceDirect

Mechanism and Machine Theory

journal homepage: www.elsevier.com/locate/mechmt

Research paper

High-order kinematics of uniform flexures

M. Verotti

Department of Mechanical, Energy, Management and Transportation Engineering, University of Genova, Via all'Opera Pia, 15 16145 Genoa, Italy

ARTICLE INFO

Keywords:
Compliant mechanisms
Flexures
Instantaneous geometric invariants
Kinematics

ABSTRACT

In the last decades, many efforts have been made to analyze and model small and large deflections of flexures, considering complex load cases and different solution techniques. However, few investigations focused on the kinematic aspects related to the deflection analysis of the flexible elements, and limited the study to the second-order kinematics. In this paper, an analytical formulation based on the instantaneous geometric invariants is developed to give deep kinematic insight, up to the fourth order, into the motion generated by the deflections. The problem is addressed from a geometrical point of view, defining the fundamental geometric entities that characterize the motion, that are inflection circle, cubic of stationary curvature and its derivative, Ball's point, and Burmester's points. Thanks to these special points on the plane, straight and circular paths can be approximated to the third and to the fourth order, respectively. The proposed formulation defines the geometric characteristics of flexures with different curvatures. An application regarding the definition of pseudo-rigid body models is discussed. Finite element simulations are performed to validate the results.

1. Introduction

Compliant mechanisms are extensively employed in many industrial and scientific fields. This increasing trend can be explained by considering their advantages over the traditional rigid-body mechanisms, consisting of performance improvement and of cost reduction [1]. Several implementations can be found in micropositioning and micromanipulation [2–4], precision machining and manufacturing [5,6], MEMS [7,8], aerospace [9–11], robotics [12–14], and lithography [15–17] applications.

Compliant mechanisms transmit force, motion, and energy through the elastic deformations of their flexible parts. In their simplest form, these parts consist of straight or curved beams [18–20] and notch hinges [21–23]. As a fundamental feature of mechanical systems, deflections of uniform or variable cross-section beams, with straight or initially-curved axis, have been studied for decades.

In the case of small deflections, elastic beam theory [24,25], Castigliano's theorems [26–28], and the principle of virtual work [29,30] proved to be useful tools for the analysis problems.

Regarding large deflections, the first contributions focused on straight or curved cantilever beams subject to concentrated or distributed loads [31–34]. More recently, different load conditions, as follower forces or combined loads, and several solution approaches, as integral and direct nonlinear solutions [35–40], and energy-based frameworks [41], have been implemented. With respect to compliant mechanisms, large deflections problems are often solved by resorting to elliptic integral solutions [42,43], beam, chained beam, and body-frame beam constraint models [44–46].

It is worth noting that large deflection analysis is a necessary prerequisite for the determination of the pseudo-rigid body model. Firstly developed by Howell and Midha [47,48], this model consists of replacing the flexible beam with two rigid links connected

E-mail address: matteo.verotti@unige.it.

https://doi.org/10.1016/j.mechmachtheory.2024.105631
Received 5 February 2024; Received in revised form 12 March 2024; Accepted 12 March 2024
Available online 16 March 2024

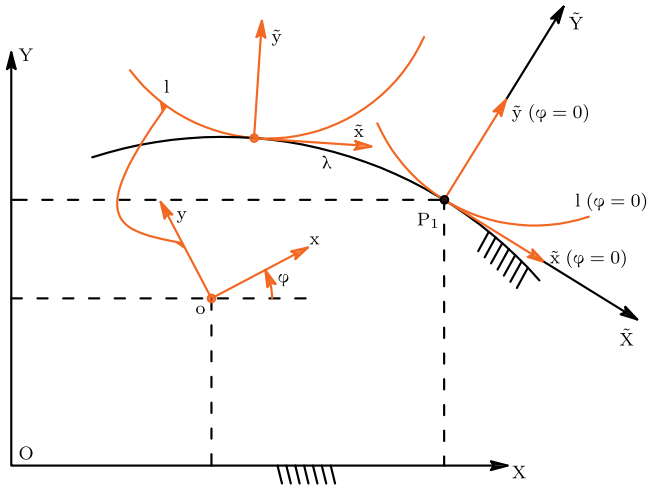

Fig. 1. Reference frames.

by a revolute joint with a torsional spring. The revolute pair position is determined by minimizing the tip error. Successively, other models with one [49] or more [50–55] kinematic pairs have been proposed. It is worth noting that PRBMs can also be adopted for the solution of synthesis problems, often addressed with topology optimization [56–58].

Although extensive efforts have been made in the analysis of the deflections, fewer studies dealt with the kinematic aspects associated to the deflection problem. The behavior of the pole of the displacements, which characterizes the rigid displacements consequent to the flexible elements motion, was first analyzed in Ref. [59,60], and exploited to formulate a pseudo-rigid-body model, based on finite displacement and strain energy, for the accurate modeling of final configurations [61]. By resorting to the instantaneous geometric invariants, Valentini and Pennestrì evaluated the centrodes and the inflection circle of the motion generated by the flexures, and developed an epicyclic pseudo-rigid-body model based on second-order kinematics [62–64].

The instantaneous geometric invariants were first introduced by Krause [65] and developed by Veldkamp [66], Bottema and Roth [67]. As powerful tools in the solution of analysis and synthesis problems, they were recently extended to the hyperbolic plane [68].

In this paper, the instantaneous geometric invariants are applied to the description of the motion generated by flexures with different curvatures. The developed analytical formulation gives kinematic insights on the geometric characteristic of motion up to the fourth order. The invariants lead to the determination of fundamental geometric entities, that are the inflection circle, the cubic of stationary curvature and its derivative, the Ball's point, and the Burmester's points. In particular, Ball's and Burmester's points identify the special points on the plane that approximate straight paths to the third order, and circular paths to the fourth order, respectively. The obtained geometric characteristics can be exploited in all the design phases, for the solution of synthesis problems with requirements of high accuracy, and for the definition of pseudo-rigid-body models.

The manuscript is organized as follows. In Section 2, the geometric invariants and the kinematic background are introduced. The motion generated by a flexure with generic initial curvature is described in Section 3, and the corresponding geometric invariants are determined in Section 4. In Section 5, the motion characteristics of two initially-curved flexures are obtained, whereas in Section 6 the particular cases of straight-axis and ring flexures are discussed. The implementation of the procedure for the definition of pseudo-rigid body models is discussed, with an example, in Section 7. Conclusions are reported in Section 8.

2. Instantaneous geometric invariants

The mathematical description of the motion is provided by considering two Cartesian reference frames, $\mathcal{F} = \{O, X, Y\}$ and $f = \{o, x, y\}$, representing the fixed and the mobile plane, respectively. With reference to Fig. 1, the motion of the mobile plane with respect to the fixed one can be described by the following relations:

$$\begin{aligned} X(t) &= X_o(t) + x\cos(\phi(t)) - y\sin(\phi(t)), \\ Y(t) &= Y_o(t) + x\sin(\phi(t)) + y\cos(\phi(t)). \end{aligned} \tag{1}$$

In case of time-based motion, X_o, Y_o, and ϕ are real functions of the parameter t (time), whereas x and y are not dependent on t. However, a geometry-based description can be introduced for the analysis of the motion properties that not depend on time. By assuming $d\phi/dt = 1$ and $\phi = 0$ for $t = 0$, it follows $t = \phi$. If ϕ is the independent variable, X_o and Y_o are function of ϕ. The generic value of ϕ is defined as *instant* and represents one position of the mobile plane with respect to the fixed one. In compact form, Eqs. (1) can be rewritten as

$$\begin{aligned} X &= X_o + x\cos\phi - y\sin\phi, \\ Y &= Y_o + x\sin\phi + y\cos\phi. \end{aligned} \tag{2}$$

The instantaneous geometric invariants are a set of parameters able to characterize the motion from a purely geometric point of view. To describe the motion, it is convenient to introduce a second pair of frames related to the fixed centrode λ and to the moving centrode l. With reference to Fig. 1, $\tilde{\mathcal{F}} = \{P_1 \tilde{X} \tilde{Y}\}$ and $\tilde{f} = \{P_1 \tilde{x} \tilde{y}\}$ are the fixed and moving canonical frames associated to λ and l, respectively. At the reference configuration, for $\phi = 0$, the frames are coincident. Regarding $\tilde{\mathcal{F}}$, its origin P_1 is the instantaneous center of rotation, the $\tilde{X}$-axis is tangent to the centrodes in P_1, and the $\tilde{Y}$-axis is oriented towards the inflection pole.

During the motion, f moves with respect to $\mathcal{F}$ and $\tilde{f}$ rolls on $\tilde{\mathcal{F}}$. As described below, the introduction of the canonical frames leads to an advantageous mathematical description of the geometric entities that characterize the motion.

The instantaneous geometric invariants are defined as

$$a_n = \frac{d^{(n)}\tilde{X}_1}{d\phi^n}, \qquad b_n = \frac{d^{(n)}\tilde{Y}_1}{d\phi^n}. \tag{3}$$

Eqs. (3) represent the n-order derivatives of the coordinates $\tilde{X}_1$ and $\tilde{Y}_1$ of the instantaneous center of rotation P_1 with respect to the independent variable ϕ, that defines the orientation of $\tilde{f}$ with respect to $\tilde{\mathcal{F}}$ during the motion. Considering the reference configuration ($\phi = 0$), and by introducing the notation

$$X_o^{(n)} = \frac{d^{(n)}X_o}{d\phi^n}, \qquad Y_o^{(n)} = \frac{d^{(n)}Y_o}{d\phi^n}, \tag{4}$$

the invariants can be written as

$$a_0 = b_0 = a_1 = b_1 = a_2 = 0, \tag{5}$$

$$b_2 = \sqrt{\left(X_0^{(2)} + Y_0^{(1)}\right)^2 + \left(Y_0^{(2)} - X_0^{(1)}\right)^2}, \tag{6}$$

$$a_3 = \frac{1}{b_2}\left(\left(X_0^{(3)} + X_0^{(1)}\right)\left(Y_0^{(2)} - X_0^{(1)}\right) - \left(Y_0^{(3)} + Y_0^{(1)}\right)\left(X_0^{(2)} + Y_0^{(1)}\right)\right), \tag{7}$$

$$b_3 = \frac{1}{b_2}\left(\left(X_0^{(3)} + X_0^{(1)}\right)\left(X_0^{(2)} + Y_0^{(1)}\right) + \left(Y_0^{(3)} + Y_0^{(1)}\right)\left(Y_0^{(2)} - X_0^{(1)}\right)\right), \tag{8}$$

$$a_4 = \frac{1}{b_2}\left(\left(X_0^{(4)} - Y_0^{(1)}\right)\left(Y_0^{(2)} - X_0^{(1)}\right) - \left(Y_0^{(4)} + X_0^{(1)}\right)\left(X_0^{(2)} + Y_0^{(1)}\right)\right), \tag{9}$$

$$b_4 = \frac{1}{b_2}\left(\left(X_0^{(4)} - Y_0^{(1)}\right)\left(X_0^{(2)} + Y_0^{(1)}\right) + \left(Y_0^{(4)} + X_0^{(1)}\right)\left(Y_0^{(2)} - X_0^{(1)}\right)\right). \tag{10}$$

As a result, the position and the geometric derivatives for the path of the generic point P, in the canonical frame $\tilde{\mathcal{F}}$ at the instant $\phi = 0$, are

$$\tilde{X}_P = \tilde{x}, \qquad \tilde{Y}_P = \tilde{y}, \tag{11}$$

$$\tilde{X}_P^{(1)} = -\tilde{y}, \qquad \tilde{Y}_P^{(1)} = \tilde{x}, \tag{12}$$

$$\tilde{X}_P^{(2)} = -\tilde{x}, \qquad \tilde{Y}_P^{(2)} = b_2 - \tilde{y}, \tag{13}$$

$$\tilde{X}_P^{(3)} = a_3 + \tilde{y}, \qquad \tilde{Y}_P^{(3)} = b_3 - \tilde{x}, \tag{14}$$

$$\tilde{X}_P^{(4)} = a_4 + \tilde{x}, \qquad \tilde{Y}_P^{(4)} = b_4 + \tilde{y}. \tag{15}$$

The previous assumptions lead to a convenient description of the geometric characteristic of the motion. Firstly, the curvature of the trajectory of point P, defined as

$$\kappa = \frac{\tilde{X}_P^{(1)}\tilde{Y}_P^{(2)} - \tilde{X}_P^{(2)}\tilde{Y}_P^{(1)}}{\left(\tilde{X}_P^{(1)^2} + \tilde{Y}_P^{(1)^2}\right)^{\frac{3}{2}}}, \tag{16}$$

can be rewritten by making use of Eqs. (12) and (13), obtaining

$$\kappa = \frac{\tilde{x}^2 + \tilde{y}^2 - b_2\tilde{y}}{\left(\tilde{x}^2 + \tilde{y}^2\right)^{\frac{3}{2}}}. \tag{17}$$

Therefore, the radius of curvature, ρ, and the position of the center of curvature, Ω, are given by

$$\rho = \frac{1}{\kappa} = \frac{\left(\tilde{x}^2 + \tilde{y}^2\right)^{\frac{3}{2}}}{\tilde{x}^2 + \tilde{y}^2 - b_2\tilde{y}} \tag{18}$$

and

$$\tilde{x}_\Omega = -\frac{b_2\tilde{x}\tilde{y}}{\tilde{x}^2 + \tilde{y}^2 - b_2\tilde{y}}, \qquad \tilde{y}_\Omega = -\frac{b_2\tilde{y}^2}{\tilde{x}^2 + \tilde{y}^2 - b_2\tilde{y}}, \tag{19}$$

respectively. From Eq. (16) or Eq. (17), it can be noted that, if

$$\tilde{X}_P^{(1)}\tilde{Y}_P^{(2)} - \tilde{X}_P^{(2)}\tilde{Y}_P^{(1)} = 0, \tag{20}$$

or

$$\tilde{x}^2 + \tilde{y}^2 - b_2\tilde{y} = 0, \tag{21}$$

the radius of curvature tends to infinity. Eq. (20) and Eq. (21) represent the equation of the inflection circle, that is the locus of points with zero normal acceleration. From the definition of curvature, it is also possible to find the locus of the points on the moving plane with stationary curvature. These points can be found, at $\phi = 0$, by imposing

$$\left.\frac{d\kappa}{d\theta}\right|_{\phi=0} = 0. \tag{22}$$

Therefore, the differentiation of Eq. (16) yields

$$\left(\tilde{X}_P^{(1)}\tilde{Y}_P^{(3)} - \tilde{X}_P^{(3)}\tilde{Y}_P^{(1)}\right)\left(\tilde{X}_P^{I^2} + \tilde{Y}_P^{I^2}\right)^{\frac{3}{2}} - 3\left(\tilde{X}_P^{(1)}\tilde{Y}_P^{(2)} - \tilde{X}_P^{(2)}\tilde{Y}_P^{(1)}\right)\left(\tilde{X}_P^{(1)}\tilde{X}_P^{(2)} - \tilde{Y}_P^{(1)}\tilde{Y}_P^{(2)}\right)\left(\tilde{X}_P^{I^2} + \tilde{Y}_P^{I^2}\right)^{\frac{1}{2}} = 0, \tag{23}$$

and, by substituting Eqs. (12)–(14) in Eq. (23), it follows

$$(\tilde{y}^2 + \tilde{x}^2)(a_3\tilde{x} + b_3\tilde{y}) + 3\tilde{x}b_2(\tilde{x}^2 + \tilde{y}^2 - b_2\tilde{y}) = 0, \tag{24}$$

that is the equation of the cubic of stationary curvature. Furthermore, by calculating the second derivative of Eq. (16), and considering Eqs. (12)–(15), it follows

$$c_4(\tilde{y}^2\tilde{x} + \tilde{x}^3) + c_1(\tilde{y}^3 + \tilde{y}\tilde{x}^2) + c_5\tilde{x}^2 + c_6\tilde{x}\tilde{y} + c_2\tilde{y}^2 + c_3\tilde{y} = 0, \tag{25}$$

where $c_1 = 5b_2 + 4a_3 - b_4$, $c_2 = -4a_3b_2 - 9b_2^2$, $c_3 = 3b_2^3$, $c_4 = -a_4 - 4b_3$, $c_5 = -3b_2^2$, $c_6 = 4b_2b_3$. Eq. (25) is the derivative of the cubic of stationary curvature. The real solutions of the system composed of Eqs. (24) and (25) give the coordinates of the Burmester points, which are points with a trajectory that, for four infinitesimal, subsequent rotations of the mobile plane, have five contact points with the osculating circle.

The instantaneous geometric invariants allow also the determination of a special point on the mobile plane, called Ball's point, defined as the intersection of the cubic of stationary curvature with the inflection circle (other than the velocity pole).

Considering Eqs. (21) and (24), its coordinates are given by

$$\tilde{x} = -b_3\frac{b_2a_3}{a_3^2 + b_3^2}, \qquad \tilde{y} = a_3\frac{b_2a_3}{a_3^2 + b_3^2}. \tag{26}$$

For three infinitesimal, subsequent rotations of the mobile plane, the trajectory of the Ball's point has four contact points with a straight line.

3. Motion description

For a constant-curvature beam, under the Euler–Bernoulli assumptions, the moment–curvature relation can be written as

$$\frac{d\theta}{ds} = \frac{1}{r} + \frac{M}{EI}, \tag{27}$$

where s is the arc-length coordinate, $d\theta/ds$ is the curvature, r is the initial radius of the beam axis, M is the internal bending moment, and EI is the bending stiffness. If l is the length of the beam, the previous equation can be rewritten as

$$\frac{d\theta}{ds} = \frac{1}{l}(2\alpha + \phi), \tag{28}$$

where

$$\alpha = \frac{l}{2r} \qquad \text{and} \qquad \phi = \frac{M}{EI}l. \tag{29}$$

In the present investigation, ϕ is assumed to be constant with respect to s, as in the case of uniform, linear elastic cantilevers subject to moments applied to the free-end section.

Fig. 2 shows the elastic element, in neutral and deflected configurations, and the fixed and mobile reference frames. The origin O of the fixed frame $\mathcal{F}\{O, X, Y\}$ is coincident to the anchored end of the beam axis, and the Y-axis is collinear to the axis chord $\overline{OE}$. The mobile frame $f\{o, x, y\}$ has origin o coincident to the free-end E of the beam axis. For $\phi = 0$, the frames f and $\mathcal{F}$ have the same orientation.

At the generic instant ϕ, the position and the orientation of the mobile frame with respect to the fixed one can be determined from Eq. (28), by separating variables, using the chain rule of differentiation, and integrating, as

$$\int_{\theta_0}^{\theta_F} d\theta = \frac{2\alpha + \phi}{l}\int_0^l ds, \tag{30}$$

$$\int_0^{X_F} dX = \frac{l}{2\alpha + \phi}\int_{\theta_0}^{\theta_F} \cos\theta d\theta, \tag{31}$$

$$\int_0^{Y_F} dY = \frac{l}{2\alpha + \phi}\int_{\theta_0}^{\theta_F} \sin\theta d\theta. \tag{32}$$

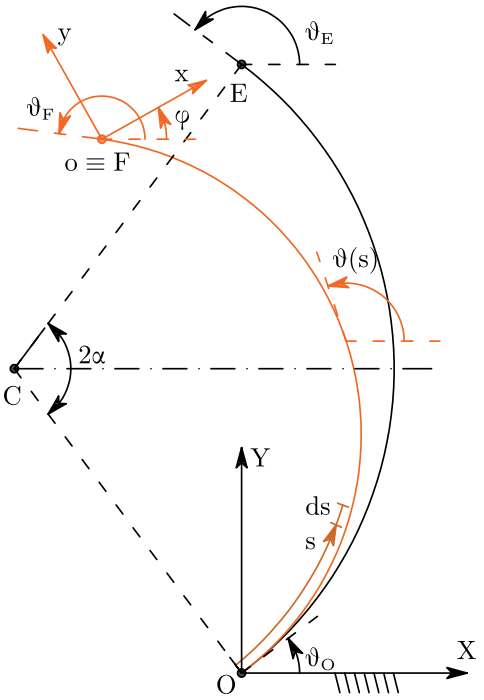

Fig. 2. Reference frames.

With reference to Fig. 2, by considering that the orientation of the anchored section is

$$\theta_O = \frac{\pi}{2} - \alpha, \tag{33}$$

Eqs. (30)–(32) become

$$\theta_F = \frac{\pi}{2} + \alpha + \phi, \tag{34}$$

$$X_F = \frac{\cos(\alpha+\phi) - \cos\alpha}{2\alpha+\phi}\, l, \tag{35}$$

$$Y_F = \frac{\sin\alpha + \sin(\alpha+\phi)}{2\alpha+\phi}\, l. \tag{36}$$

According to the notation introduced in Section 2, the non-dimensional coordinates

$$X_0 = \frac{X_F}{l} \quad \text{and} \quad Y_0 = \frac{Y_F}{l} \tag{37}$$

are considered for the evaluation of the geometric invariants.

4. Determination of the instantaneous geometric invariants

To define the geometric invariants, the first step consists of calculating the coordinates of the mobile frame $f\{o, x, y\}$, having origin coincident to the free end of the beam axis. The coordinates given by Eqs. (35) and (36) can be written, in non-dimensional form according to Eq. (37), as

$$X_0 = \frac{\cos(\alpha+\phi) - \cos(\alpha)}{2\alpha+\phi}, \tag{38}$$

$$Y_0 = \frac{\sin(\alpha) + \sin(\alpha+\phi)}{2\alpha+\phi}. \tag{39}$$

The derivatives of Eqs. (38) and (39) with respect to the independent variable ϕ, introduced in Eq. (4), are

$$X_0^{(1)} = -\frac{\cos(\alpha+\phi) - \cos(\alpha)}{(2\alpha+\phi)^2} - \frac{\sin(\alpha+\phi)}{2\alpha+\phi}, \tag{40}$$

$$Y_0^{(1)} = -\frac{\sin(\alpha) + \sin(\alpha+\phi)}{(2\alpha+\phi)^2} + \frac{\cos(\alpha+\phi)}{2\alpha+\phi}, \tag{41}$$

$$X_0^{(2)} = \frac{2\cos(\alpha+\phi) - 2\cos(\alpha)}{(2\alpha+\phi)^3} + \frac{2\sin(\alpha+\phi)}{(2\alpha+\phi)^2} - \frac{\cos(\alpha+\phi)}{2\alpha+\phi}, \tag{42}$$

$$Y_0^{(2)} = \frac{2\sin(\alpha) + 2\sin(\alpha+\phi)}{(2\alpha+\phi)^3} - \frac{2\cos(\alpha+\phi)}{(2\alpha+\phi)^2} - \frac{\sin(\alpha+\phi)}{2\alpha+\phi}, \tag{43}$$

$$X_0^{(3)} = -\frac{6(\cos(\alpha+\phi) - \cos(\alpha))}{(2\alpha+\phi)^4} - \frac{6\sin(\alpha+\phi)}{(2\alpha+\phi)^3} + \frac{3\cos(\alpha+\phi)}{(2\alpha+\phi)^2} + \frac{\sin(\alpha+\phi)}{2\alpha+\phi}, \tag{44}$$

$$Y_0^{(3)} = -\frac{6(\sin(\alpha) + \sin(\alpha+\phi))}{(2\alpha+\phi)^4} + \frac{6\cos(\alpha+\phi)}{(2\alpha+\phi)^3} + \frac{3\sin(\alpha+\phi)}{(2\alpha+\phi)^2} - \frac{\cos(\alpha+\phi)}{2\alpha+\phi}, \tag{45}$$

$$X_0^{(4)} = \frac{24\cos(\alpha+\phi) - 24\cos(\alpha)}{(2\alpha+\phi)^5} + \frac{24\sin(\alpha+\phi)}{(2\alpha+\phi)^4} - \frac{12\cos(\alpha+\phi)}{(2\alpha+\phi)^3} - \frac{4\sin(\alpha+\phi)}{(2\alpha+\phi)^2} + \frac{\cos(\alpha+\phi)}{2\alpha+\phi}, \tag{46}$$

$$Y_0^{(4)} = \frac{24\sin(\alpha) + 24\sin(\alpha+\phi)}{(2\alpha+\phi)^5} - \frac{24\cos(\alpha+\phi)}{(2\alpha+\phi)^4} - \frac{12\sin(\alpha+\phi)}{(2\alpha+\phi)^3} + \frac{4\cos(\alpha+\phi)}{(2\alpha+\phi)^2} + \frac{\sin(\alpha+\phi)}{2\alpha+\phi}. \tag{47}$$

Then, by substituting Eqs. (40)–(47) in Eqs. (6)–(10), the instantaneous geometric invariants are obtained as follows:

$$b_2 = \frac{\sqrt{2}}{(2\alpha+\phi)^3}\left((\phi+2\alpha+2)(\phi+2\alpha-2)\cos(2\alpha+\phi) - (8\alpha+4\phi)\sin(2\alpha+\phi) + \phi^2 + 4\alpha\phi + 4\alpha^2 + 4\right)^{\frac{1}{2}}, \tag{48}$$

$$a_3 = \frac{1}{b_2(2\alpha+\phi)^6}\left(-3(\phi+2\alpha+2)(\phi+2\alpha-2)\cos(2\alpha+\phi) + (24\alpha+12\phi)\sin(2\alpha+\phi) - 3\phi^2 - 12\alpha\phi - 12\alpha^2 - 12\right), \tag{49}$$

$$\begin{aligned} b_3 = {} & \frac{1}{b_2(2\alpha+\phi)^7}\left(-(2\alpha+\phi)\left(4\alpha^2 + 4\alpha\phi + \phi^2 - 24\right)\sin(2\alpha+\phi)\right. \\ & \left. + \left(-32\alpha^2 - 32\alpha\phi - 8\phi^2 + 24\right)\cos(2\alpha+\phi) - 4\phi^2 - 16\alpha\phi - 16\alpha^2 - 24\right), \end{aligned} \tag{50}$$

$$\begin{aligned} a_4 = {} & \frac{1}{b_2(2\alpha+\phi)^7}\left(2(2\alpha+\phi)\left(4\alpha^2 + 4\alpha\phi + \phi^2 - 24\right)\sin(2\alpha+\phi) + \right. \\ & \left. \left(64\alpha^2 + 64\alpha\phi + 16\phi^2 - 48\right)\cos(2\alpha+\phi) + 8\phi^2 + 32\alpha\phi + 32\alpha^2 + 48\right), \end{aligned} \tag{51}$$

$$\begin{aligned} b_4 = {} & \frac{1}{b_2(2\alpha+\phi)^8}\left(\left(-64\alpha^4 - 128\alpha^3\phi + \left(-96\phi^2 + 192\right)\alpha^2 \right. \right. + \left(-32\phi^3 + 192\phi\right)\alpha - 4\phi^4 + 48\phi^2 - 96\Big)\cos(2\alpha+\phi) \\ & \left. +20(2\alpha+\phi)\left(\phi^2 + 4\alpha\phi + 4\alpha^2 - \frac{24}{5}\right)\sin(2\alpha+\phi) \right. -4\phi^4 - 32\alpha\,\phi^3 - 96\alpha^2\phi^2 - 128\alpha^3\phi - 64\alpha^4 + 96\Big). \end{aligned} \tag{52}$$

In the next Section, the geometric invariants will be exploited to describe the geometric characteristics of the motion of flexures with different curvatures.

5. Motion characteristic of constant curvature flexures

By resorting to the geometric invariants, the motion of flexures with unit length axis and initial curvature $\rho = 2\alpha$, with $\alpha = \pi/4$ and $\alpha = \pi/2$, is examined.

5.1. Curved flexure, $\alpha = \pi/4$

In case of $\alpha = \pi/4$ at $\phi = 0$, the geometric invariants become

$$b_2 = \frac{16\sqrt{2}}{\pi^3} - \frac{4\sqrt{2}}{\pi^2}, \tag{53}$$

$$a_3 = \frac{6\sqrt{2}(\pi-4)}{\pi^3}, \tag{54}$$

$$b_3 = \frac{2\sqrt{2}\left(\pi^2 + 12\pi - 48\right)}{\pi^4}, \tag{55}$$

$$a_4 = -\frac{4\sqrt{2}\left(\pi^2 + 12\pi - 48\right)}{\pi^4}, \tag{56}$$

$$b_4 = \frac{8\sqrt{2}\left(\pi^3 - 6\pi^2 - 24\pi + 96\right)}{\pi^5}. \tag{57}$$

According to the approach described in Section 2, Eqs. (53)–(57) allow the determination of the following geometrical entities in the canonical reference.

- Inflection circle (Eq. (21)):

$$\tilde{x}^2 - \left(\frac{16\sqrt{2}}{\pi^3} - \frac{4\sqrt{2}}{\pi^2}\right)\tilde{y} - \tilde{y}^2 = 0. \tag{58}$$

- Cubic of stationary curvature (Eq. (24)):

$$8\tilde{x}\tilde{y}\left(\pi-4\right)^2\sqrt{2}+\left(\left(\tilde{x}-\frac{\tilde{y}}{3}\right)\pi^2+\left(-4\tilde{x}-4\tilde{y}\right)\pi+16\tilde{y}\right)\left(\tilde{y}^2+\tilde{x}^2\right)\pi^2=0. \tag{59}$$

- Derivative of the cubic of stationary curvature (Eq. (25)):

$$\begin{aligned}&12\left(\left(\tilde{x}^2+\frac{2}{3}\tilde{y}\tilde{x}+\tilde{y}^2\right)\pi^2-4\left(\tilde{x}-\tilde{y}\right)^2\pi-32\tilde{y}\tilde{x}\right)\left(\pi-4\right)\pi^2\sqrt{2}+\left(\tilde{x}+\tilde{y}\right)\left(\tilde{y}^2+\tilde{x}^2\right)\pi^7+12\left(\tilde{y}^2+\tilde{x}^2\right)\left(\tilde{x}-\frac{2\tilde{y}}{3}\right)\pi^6-\\&48\left(\tilde{x}+\tilde{y}\right)\left(\tilde{y}^2+\tilde{x}^2\right)\pi^5+\left(192\tilde{y}^3+192\tilde{x}^2\tilde{y}\right)\pi^4+96\pi^3\tilde{y}-1152\pi^2\tilde{y}+4608\pi\tilde{y}-6144\tilde{y}=0.\end{aligned} \tag{60}$$

- Burmester's points (Eqs. (24) and (25)) and corresponding center of curvature (Eq. (19)):

$$B_u=\{\ \ 0.1095\,;\,0.3402\}\,,\qquad \Omega=\{-0.0783\,;\,-0.2435\} \tag{61}$$

$$B_u=\{-0.0783\,;\,0.2435\}\,,\qquad \Omega=\{\ \ 0.1094\,;\,-0.3402\} \tag{62}$$

- Ball's point (Eq. (26)):

$$B_a=\{-0.0083\,;\,0.1562\}\,. \tag{63}$$

The pole of velocity, the fixed and moving centrodes, and the canonical reference are depicted in Fig. 3(a). Inflection circle, cubic of stationary curvature and its derivative, Burmester's points and Ball's point are reported in Fig. 3(b). The trajectories of the Burmester's points and their osculating circles, and the trajectory of the Ball's point and its corresponding straight line to be approximated, are shown in Fig. 3(c).

5.2. Curved flexure, $\alpha=\pi/2$

Considering $\alpha=\pi/2$ at the instant $\phi=0$, the geometric invariants Eqs. (49) and (49)–(52) take the form

$$b_2=\frac{4}{\pi^3}, \tag{64}$$

$$a_3=-\frac{6}{\pi^3}, \tag{65}$$

$$b_3=-\frac{12}{\pi^4}+\frac{1}{\pi^2}, \tag{66}$$

$$a_4=\frac{24}{\pi^4}-\frac{2}{\pi^2}, \tag{67}$$

$$b_4=\frac{48}{\pi^5}-\frac{12}{\pi^3}. \tag{68}$$

Following the procedure in Section 5.1, the geometrical entities of motion are obtained as follows.

- Inflection circle (Eq. (21)):

$$\tilde{x}^2-\frac{4}{\pi^3}\tilde{y}-\tilde{y}^2=0. \tag{69}$$

- Cubic of stationary curvature (Eq. (24)):

$$\pi^4\tilde{y}^3+\pi^4\tilde{y}\,\tilde{x}^2+6\pi^3\tilde{y}^2\tilde{x}+6\pi^3\tilde{x}^3-12\pi^2\tilde{y}^3-12\pi^2\tilde{y}\,\tilde{x}^2-48\tilde{y}\tilde{x}=0. \tag{70}$$

- Derivative of the cubic of stationary curvature (Eq. (25)):

$$2\left(12-\pi^2\right)\left(\tilde{y}^2+\tilde{x}^2\right)\tilde{x}+\frac{8\left(\pi^2-6\right)\left(\tilde{y}^2+\tilde{x}^2\right)\tilde{y}}{\pi}-\frac{48\tilde{x}^2}{\pi^2}+\frac{16\left(\pi^2-12\right)\tilde{x}\tilde{y}}{\pi^3}-\frac{48\tilde{y}^2}{\pi^2}+\frac{192\tilde{y}}{\pi^5}=0. \tag{71}$$

- Burmester's points (Eqs. (24) and (25)) and corresponding center of curvature (Eq. (19)):

$$B_u=\{-0.0733\,;\,0.1726\}\,,\qquad \Omega=\{\ \ 0.1265\,;\,-0.2979\} \tag{72}$$

$$B_u=\{\ \ 0.1265\,;\,0.2979\}\,,\qquad \Omega=\{-0.0733\,;\,-0.1726\} \tag{73}$$

- Ball's point (Eq. (26)):

$$B_a=\{-0.0144\,;\,0.1274\}\,. \tag{74}$$

The geometric entities are reported in Fig. 4.

6. Particular cases: straight-axis and ring flexures

Two particular cases are considered, consisting of the motion analysis of the straight-axis flexure and of the ring flexure, corresponding to $\alpha=0$ and $\alpha=\pi$, respectively.

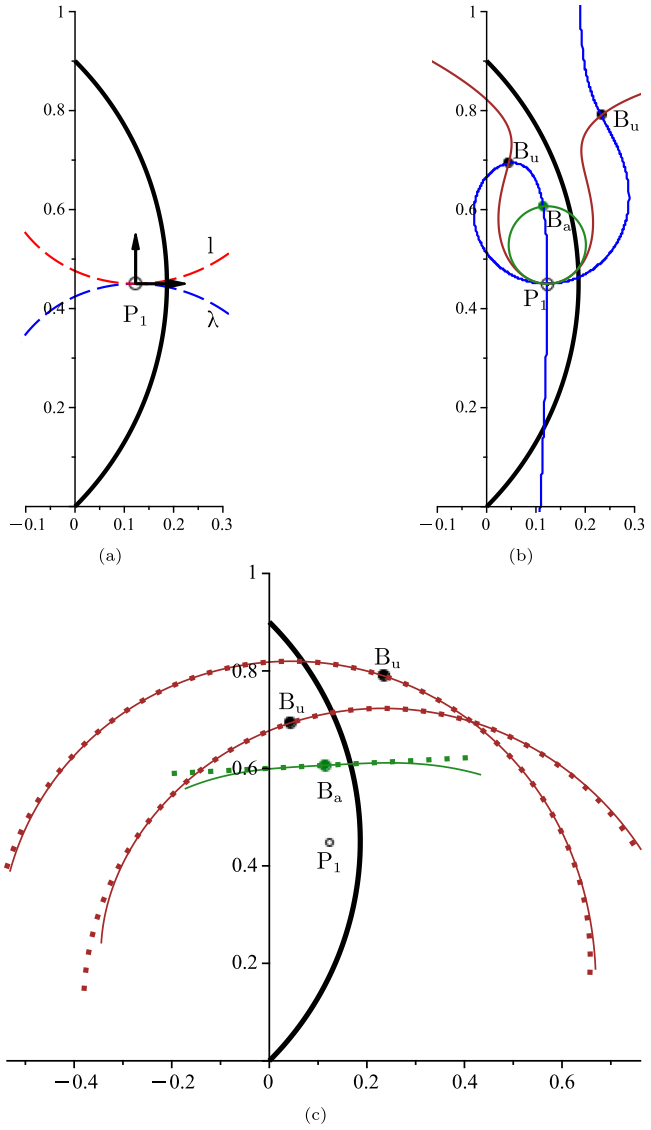

Fig. 3. Kinematics of the curved flexure with $\alpha = \pi/4$. (a) Fixed (blue) and moving (red) centrodes, and canonical reference; (b) inflection circle (green), cubic of stationary curvature (blue) and its derivative (red), Burmester's points trajectories (solid red) and osculating circles (dot red), Ball's point trajectory (solid green) and straight line (dot green). (For interpretation of the references to color in this figure legend, the reader is referred to the web version of this article.)

6.1. *Straight-axis flexure,* $\alpha = 0$

In the case of $\alpha = 0$, the coordinates of the origin of the mobile frame and its geometric derivatives reported in Eqs. (40)–(47) become

$$X_0 = \frac{\cos(\phi) - 1}{\phi}, \tag{75}$$

$$Y_0 = \frac{\sin(\phi)}{\phi}, \tag{76}$$

$$X_0^{(1)} = -\frac{\cos(\phi) - 1}{\phi^2} - \frac{\sin(\phi)}{\phi}, \tag{77}$$

$$Y_0^{(1)} = -\frac{\sin(\phi)}{\phi^2} + \frac{\cos(\phi)}{\phi}, \tag{78}$$

$$X_0^{(2)} = \frac{2\cos(\phi) - 2}{\phi^3} + \frac{2\sin(\phi)}{\phi^2} - \frac{\cos(\phi)}{\phi}, \tag{79}$$

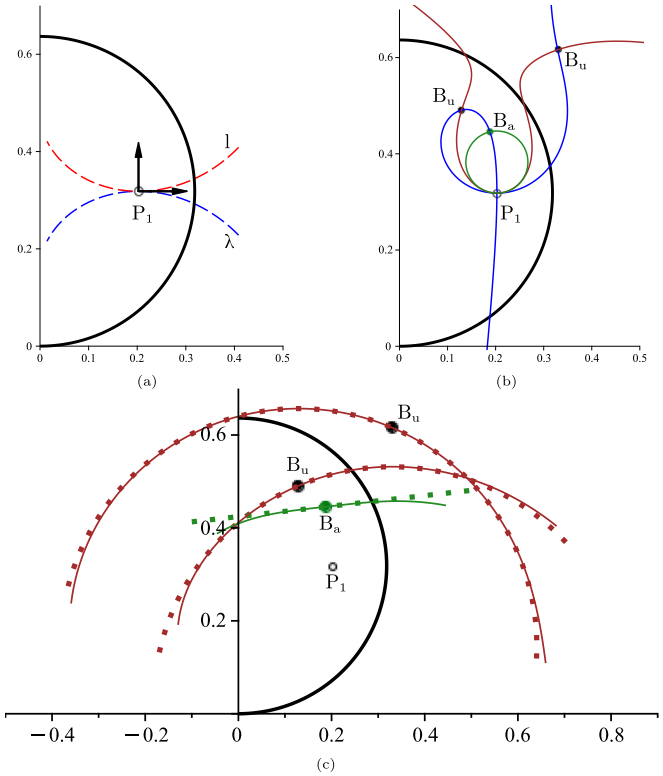

Fig. 4. Kinematics of the curved flexure with $\alpha = \pi/2$. (a) Fixed (blue) and moving (red) centrodes, and canonical reference; (b) inflection circle (green), cubic of stationary curvature (blue) and its derivative (red), Burmester's points trajectories (solid red) and osculating circles (dot red), Ball's point trajectory (solid green) and straight line (dot green). (For interpretation of the references to color in this figure legend, the reader is referred to the web version of this article.)

$$Y_0^{(2)} = \frac{2\sin(\phi)}{\phi^3} - \frac{2\cos(\phi)}{\phi^2} - \frac{\sin(\phi)}{\phi}, \tag{80}$$

$$X_0^{(3)} = -\frac{6(\cos(\phi)-1)}{\phi^4} - \frac{6\sin(\phi)}{\phi^3} + \frac{3\cos(\phi)}{\phi^2} + \frac{\sin(\phi)}{\phi}, \tag{81}$$

$$Y_0^{(3)} = -\frac{6\sin(\phi)}{\phi^4} + \frac{6\cos(\phi)}{\phi^3} + \frac{3\sin(\phi)}{\phi^2} - \frac{\cos(\phi)}{\phi}, \tag{82}$$

$$X_0^{(4)} = \frac{24\cos(\phi)-24}{\phi^5} + \frac{24\sin(\phi)}{\phi^4} - \frac{12\cos(\phi)}{\phi^3} - \frac{4\sin(\phi)}{\phi^2} + \frac{\cos(\phi)}{\phi}, \tag{83}$$

$$Y_0^{(4)} = \frac{24\sin(\phi)}{\phi^5} - \frac{24\cos(\phi)}{\phi^4} - \frac{12\sin(\phi)}{\phi^3} + \frac{4\cos(\phi)}{\phi^2} + \frac{\sin(\phi)}{\phi}. \tag{84}$$

The geometric invariants defined in Eqs. (49) and (49)–(52), for $\alpha = 0$ take the following form:

$$b_2 = \frac{1}{\phi^3}\sqrt{2\phi^2(\cos(\phi)+1) - 8(\sin(\phi)\phi + \cos(\phi) - 1)}, \tag{85}$$

$$a_3 = \frac{1}{b_2\phi^6}\left(-3\cos(\phi)\phi^2 + 12\sin(\phi)\phi - 3\phi^2 + 12\cos(\phi) - 12\right), \tag{86}$$

$$b_3 = \frac{1}{b_2\phi^7}\left(\left(-\phi^3 + 24\phi\right)\sin(\phi) - 8\cos(\phi)\phi^2 - 4\phi^2 + 24\cos(\phi) - 24\right), \tag{87}$$

$$a_4 = \frac{1}{b_2\phi^7}\left(\left(2\phi^3 - 48\phi\right)\sin(\phi) + 16\cos(\phi)\phi^2 + 8\phi^2 - 48\cos(\phi) + 48\right), \tag{88}$$

$$b_4 = \frac{1}{b_2\phi^8}\left(\left(20\phi^3 - 96\phi\right)\sin(\phi) + \left(-4\phi^4 + 48\phi^2 - 96\right)\cos(\phi) - 4\phi^4 + 96\right). \tag{89}$$

According to Eqs. (85)–(89), the geometric invariants are not defined at $\phi = 0$. However, by computing the limit as ϕ tends to 0, it follows

$$\lim_{\phi\to 0} b_2 = \frac{1}{6}, \tag{90}$$

$$\lim_{\phi\to 0} a_3 = -\frac{1}{4}, \tag{91}$$

$$\lim_{\phi\to 0} b_3 = 0, \tag{92}$$

$$\lim_{\phi\to 0} a_4 = 0, \tag{93}$$

$$\lim_{\phi\to 0} b_4 = -\frac{3}{10}. \tag{94}$$

Considering the limits of the invariants, the geometrical entities of the motion can be calculated as follows.

- Inflection circle (Eq. (21)):

$$\tilde{x}^2 - \frac{1}{6}\tilde{y} - \tilde{y}^2 = 0. \tag{95}$$

- Cubic of stationary curvature (Eq. (24)):

$$\tilde{x}\left(3\tilde{y}^2 + 3\tilde{x}^2 - \tilde{y}\right) = 0. \tag{96}$$

- Derivative of the cubic of stationary curvature (Eq. (25)):

$$\frac{2}{15}\tilde{y}^3 + \frac{2}{15}\tilde{x}^2\tilde{y} - \frac{1}{12}\tilde{x}^2 - \frac{1}{12}\tilde{y}^2 + \frac{1}{72}\tilde{y} = 0. \tag{97}$$

- Burmester's points (Eqs. (24) and (25)) and corresponding center of curvature (Eq. (19)):

$$B_u = \left\{ \frac{\sqrt{15}}{48} ; \frac{5}{16} \right\}, \qquad \Omega = \left\{ -\frac{\sqrt{15}}{48} ; -\frac{5}{16} \right\} \tag{98}$$

$$B_u = \left\{ -\frac{\sqrt{15}}{48} ; \frac{5}{16} \right\}, \qquad \Omega = \left\{ \frac{\sqrt{15}}{48} ; -\frac{5}{16} \right\} \tag{99}$$

- Ball's point (Eq. (26)):

$$B_a = \left\{ 0 ; \frac{1}{6} \right\}, \tag{100}$$

The geometric entities are reported in Fig. 5. It is worth noting that the cubic of stationary curvature degenerates to a circle and a straight line, as shown in Fig. 5(b). In particular, the cubic and its derivative are symmetric with respect to the flexure axis. Also, the center of the inflection circle and the Ball's point lie on the same axis. As a consequence, the Burmester's points and their related circular paths, and the straight path associated to the Ball's point, are symmetric.

6.2. *Ring flexure, $\alpha = \pi$*

Considering $\alpha = \pi$ at the instant $\phi = 0$, the geometric invariants Eqs. (49) and (49)–(52) become

$$b_2 = \frac{1}{2\pi^2}, \tag{101}$$

$$a_3 = -\frac{3}{4\pi^2}, \tag{102}$$

$$b_3 = -\frac{3}{4\pi^3}, \tag{103}$$

$$a_4 = \frac{3}{2\pi^3}, \tag{104}$$

$$b_4 = \frac{3}{2\pi^4} - \frac{1}{\pi^2}. \tag{105}$$

Following the procedure in Section 5.1, the geometrical entities of the motion are obtained as follows.

- Inflection circle (Eq. (21)):

$$\tilde{x}^2 - \frac{1}{2\pi^2}\tilde{y} - \tilde{y}^2 = 0. \tag{106}$$

- Cubic of stationary curvature (Eq. (24)):

$$\pi^2\tilde{y}^2\tilde{x} + \pi^2\tilde{x}^3 - \pi\,\tilde{y}^3 - \pi\tilde{y}\,\tilde{x}^2 - \tilde{y}\tilde{x} = 0. \tag{107}$$

- Derivative of the cubic of stationary curvature (Eq. (25)):

$$\frac{3y^2x}{2\pi^3} + \frac{3x^3}{2\pi^3} + \left(\frac{1}{2\pi^2} - \frac{3}{2\pi^4}\right)\left(y^3 + yx^2\right) - \frac{3x^2}{4\pi^4} - \frac{3xy}{2\pi^5} - \frac{3y^2}{4\pi^4} + \frac{3y}{8\pi^6} = 0. \tag{108}$$

- Burmester's points (Eqs. (24) and (25)) and corresponding center of curvature (Eq. (19)):

$$B_u = \{\ 0.0832 ; 0.1071\}, \qquad \Omega = \{-0.0348 ; -0.0448\} \tag{109}$$

$$B_u = \{-0.0348 ; 0.0448\}, \qquad \Omega = \{\ 0.0832 ; -0.1071\} \tag{110}$$

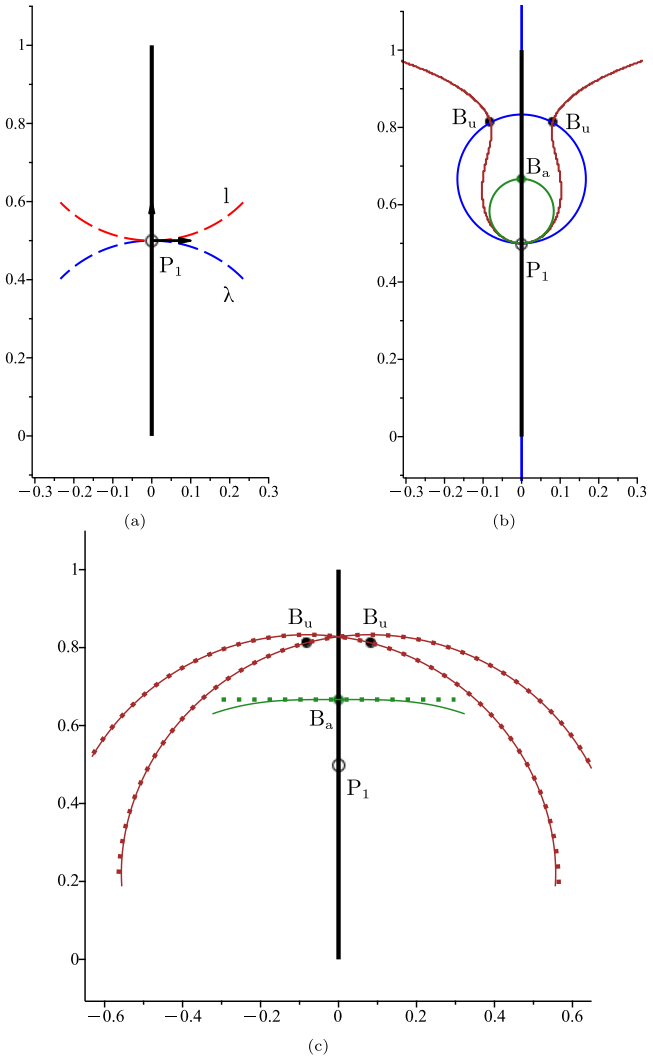

Fig. 5. Kinematics of the straight flexure, $\alpha = 0$. (a) Fixed (blue) and moving (red) centrodes, and canonical reference; (b) inflection circle (green), degenerated cubic of stationary curvature (blue) and its derivative (red), Burmester's points trajectories (solid red) and osculating circles (dot red), Ball's point trajectory (solid green) and straight line (dot green). (For interpretation of the references to color in this figure legend, the reader is referred to the web version of this article.)

- Ball's point (Eq. (26)):

$$B_a = \{-0.0146\,;\, 0.0460\}\,. \tag{111}$$

The geometric entities are reported in Fig. 6.

7. Rigid-body modeling

The procedure described in the previous sections leads to the definition of pseudo-rigid body models that reproduce with high accuracy the position of a rigid section of the flexure. Fig. 7 shows the straight-axis flexure and the Burmester's point B_u, rigidly connected to its free-end section. As demonstrated in Section 6.1, B_u is a point of the mobile plane that follows, with the fourth order of approximation, a circular path. The center of curvature of the trajectory in B_u is Ω, and the radius of curvature is $\rho = \overline{\Omega B_u}$. Therefore, the motion can be modeled by means of a rigid link, with length ρ, connected to the ground by a revolute pair with axis passing through Ω. Fig. 7 shows the flexure and its corresponding 1R PRBM in initial configurations, and after a clockwise rotation. The same procedure can be adopted for the definition of the PRBM associated to the second Burmester's point, whereas the modeling of the Ball's point requires the implementation of a prismatic pair (1P PRBM). The same reasoning can be followed for the othe flexure with initial curvature.

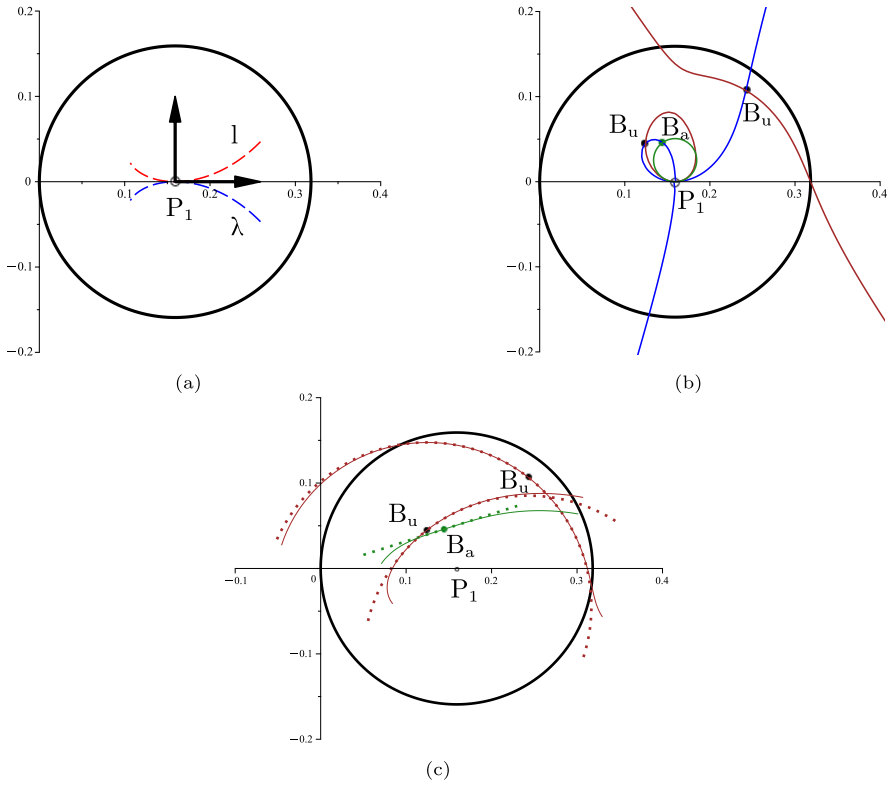

Fig. 6. Kinematics of the curved flexure with $\alpha = \pi$. (a) Fixed (blue) and moving (red) centrodes, and canonical reference; (b) inflection circle (green), cubic of stationary curvature (blue) and its derivative (red), Burmester's points trajectories (solid red) and osculating circles (dot red), Ball's point trajectory (solid green) and straight line (dot green). (For interpretation of the references to color in this figure legend, the reader is referred to the web version of this article.)

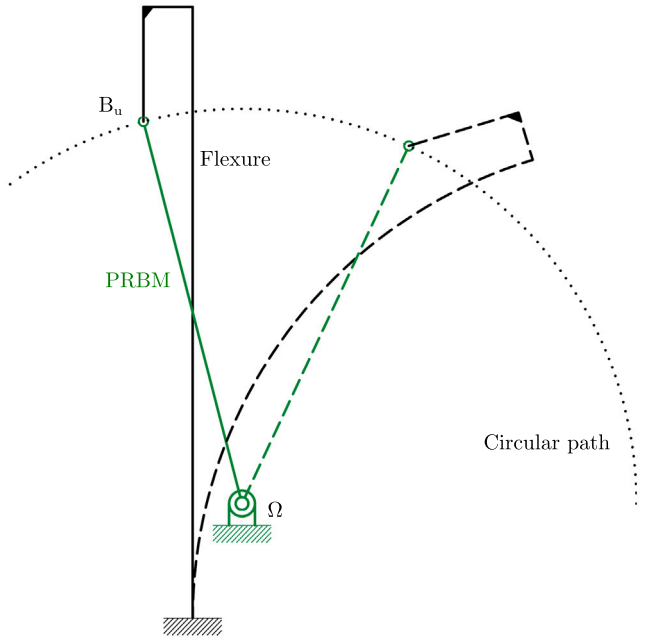

Fig. 7. Straight-axis flexure($\alpha = 0$) defining an approximating circular path through the Burmester's point B_{u1} and the corresponding PRBM. Initial and final configurations are depicted in solid and dashed lines, respectively.

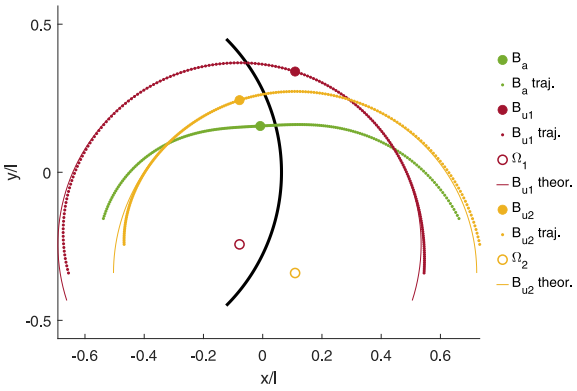

Fig. A.8. Finite element simulations for the case $\alpha = \pi/4$.

8. Conclusions

In this paper, the motion generated by flexures with initial curvature has been described resorting to the instantaneous geometric invariants. An analytical formulation has been developed to define the fundamental geometrical entities of the motion. Flexures with different curvature have been considered, including straight axis, axes subtending the angles $\pi/2$ and π, and the ring flexure (subtending the angle 2π). For each case, the equations of the inflection circle, the cubic of stationary curvature and its derivative are presented. The Ball's and Burmester's points have been determined, identifying the special points on the plane that approximate straight paths to the third order, and circular paths to the fourth order, respectively. The proposed formulation has been exploited for the definition of pseudo-rigid-body models. Theoretical results have been validated by performing a set of finite element simulations.

CRediT authorship contribution statement

M. Verotti: Writing – review & editing, Writing – original draft, Software, Methodology, Investigation, Formal analysis, Conceptualization.

Declaration of competing interest

The authors declare that they have no known competing financial interests or personal relationships that could have appeared to influence the work reported in this paper.

Data availability

No data was used for the research described in the article.

Appendix. FEA simulations

FEA simulations have been performed with the commercial software Ansys. According to the theoretical model, flexures with unit-length axis ($l = 1$) have been considered, with cross-sections having in-plane thickness and out-of-plane thickness equal to $l/20$ and $7/20$, respectively. Flexures have been meshed with 100 BEAM3 elements. The rigid connections between the free-end section and the Burmester's and Ball's points have been modeled with the multipoint constraint element MPC184. Geometric nonlinearities have been considered in the simulation setup. An increasing moment has been applied at the free-end sections, determining rotations from $-\pi$ to π. During the simulations, the trajectories of the Burmester's and Ball's points have been acquired. The trajectories corresponding to the flexure curvatures defined by $\alpha = \pi/4$, $\alpha = \pi/2$, $\alpha = 0$, and $\alpha = \pi$, are reported in Fig. A.8, Fig. A.9, Fig. A.10, and Fig. A.11, respectively. Numerical results show perfect agreement with the theoretical ones.

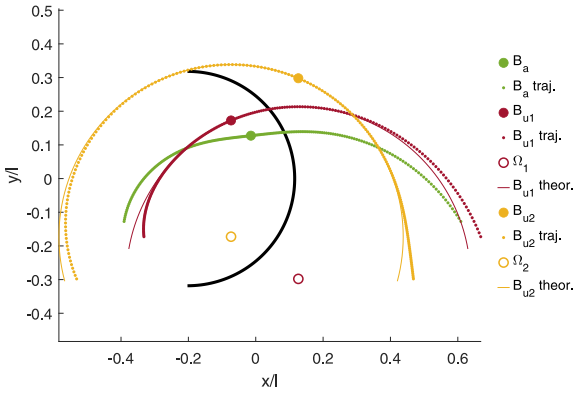

Fig. A.9. Finite element simulations for the case $\alpha = \pi/2$.

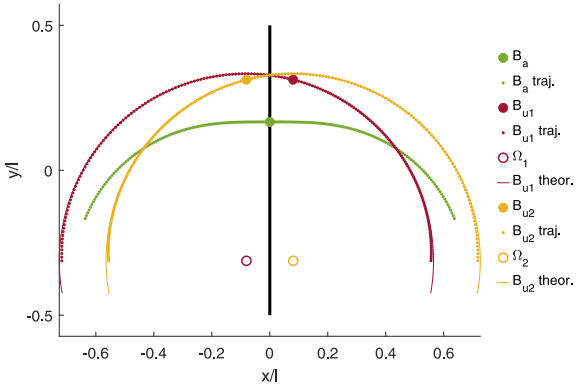

Fig. A.10. Finite element simulations for the case $\alpha = 0$.

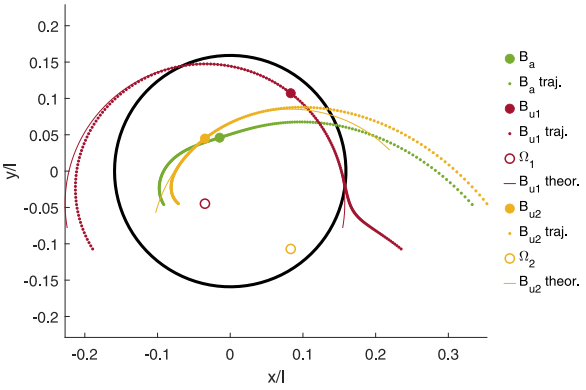

Fig. A.11. Finite element simulations for the case $\alpha = \pi$.

References

[1] L. Howell, Compliant Mechanisms, Wiley, New York, 2001.

[2] Z. Lyu, Q. Xu, L. Zhu, Design of a compliant vertical micropositioning stage based on lamina emergent mechanisms, IEEE/ASME Trans. Mechatronics 28 (4) (2023) 2131–2141, http://dx.doi.org/10.1109/TMECH.2023.3235336.

[3] Z. Guo, Z. Lyu, Q. Xu, Design of a piezoelectric-driven microgripper with three working modes, IEEE/ASME Trans. Mechatronics 9 (1) (2023) 260–270, http://dx.doi.org/10.1109/tmech.2023.3276191.

[4] A. Al-Jodah, B. Shirinzadeh, M. Ghafarian, T.K. Das, J. Pinskier, Design, modeling, and control of a large range 3-DOF micropositioning stage, Mech. Mach. Theory 156 (2021) 104159.

[5] M. Horvatek, Improved linear stage hinge design suitable for additive manufacturing, J. Mech. Sci. Technol. 37 (3) (2023) 1139–1144, http://dx.doi.org/10.1007/s12206-022-2111-5.

[6] Y. Tian, B. Shirinzadeh, D. Zhang, A flexure-based mechanism and control methodology for ultra-precision turning operation, Precis. Eng. 323 (2) (2009) 160–166.

[7] P. Schmitt, M. Hoffmann, A force-compensated compliant MEMS-amplifier with electrostatic anti-springs, Microsyst. Nanoeng. 9 (83) (2023) http://dx.doi.org/10.1038/s41378-023-00557-5.

[8] C. Joshitha, C. Santhosh, B.S. Sreeja, S. Rooban, G.S.N.K. Rao, Bistable microdevice with electrothermal compliant mechanism, Trans. Electr. Electron. Mater. 23 (3) (2021) 262–271, http://dx.doi.org/10.1007/s42341-021-00345-w.

[9] E.G. Merriam, J.E. Jones, S.P. Magleby, L.L. Howell, Monolithic 2 DOF fully compliant space pointing mechanism, Mech. Sci. 4 (2) (2013) 381–390, http://dx.doi.org/10.5194/ms-4-381-2013.

[10] W. Zeng, F. Gao, H. Jiang, C. Huang, J. Liu, H. Li, Design and analysis of a compliant variable-diameter mechanism used in variable-diameter wheels for lunar rover, Mech. Mach. Theory 125 (2018) 240–258.

[11] D. Budzyń, H. Zare-Behtash, A. Cowley, A. Cammarano, Implicit lunar dust mitigation technology: Compliant mechanisms, Acta Astronaut. 203 (2023) 146–156, http://dx.doi.org/10.1016/j.actaastro.2022.11.042.

[12] J. Yao, Y. Fang, X. Yang, P. Wang, L. Li, Design optimization of soft robotic fingers biologically inspired by the fin ray effect with intrinsic force sensing, Mech. Mach. Theory 191 (2024) 105472, http://dx.doi.org/10.1016/j.mechmachtheory.2023.105472.

[13] P. Bilancia, M. Baggetta, G. Berselli, L. Bruzzone, P. Fanghella, Design of a bio-inspired contact-aided compliant wrist, Robot. Comput.-Integr. Manuf. 67 (2021) 102028.

[14] T. Morales Bieze, A. Kruszewski, B. Carrez, C. Duriez, Design, implementation, and control of a deformable manipulator robot based on a compliant spine, Int. J. Robot. Res. 39 (14) (2020) 1604–1619.

[15] Y. Liu, Z. Zhang, A large range compliant nano-manipulator supporting electron beam lithography, J. Mech. Des. 144 (4) (2022) 043303, http://dx.doi.org/10.1115/1.4053462.

[16] K. Xu, H. Luo, J. Qin, M. Yang, S. Guo, L. Wang, Flexible devices fabricated by a plate-to-roll nanoimprint lithography system, Nanotechnology 30 (7) (2018) 075301.

[17] T.J. Teo, G. Yang, I.-M. Chen, A large deflection and high payload flexure-based parallel manipulator for UV nanoimprint lithography: Part I. Modeling and analyses, Precis. Eng. 38 (4) (2014) 861–871.

[18] F. Beyeler, A. Neild, S. Oberti, D. Bell, Y. Sun, J. Dual, B. Nelson, Monolithically fabricated microgripper with integrated force sensor for manipulating microobjects and biological cells aligned in an ultrasonic field, J. Microelectromech. Syst. 16 (1) (2007) 7–15.

[19] Y. Bellouard, Microrobotics: Methods and Applications, CRC Press, 2010.

[20] S.A. Bazaz, F. Khan, R.I. Shakoor, Design, simulation and testing of electrostatic SOI MUMPs based microgripper integrated with capacitive contact sensor, Sensors Actuators A 167 (1) (2011) 44–53.

[21] N. Lobontiu, E. Garcia, M. Goldfarb, J.S. Paine, Corner-filleted flexure hinges, Trans. ASME, J. Mech. Des. 123 (3) (2001) 346–352.

[22] Y.K. Yong, T.-F. Lu, D.C. Handley, Review of circular flexure hinge design equations and derivation of empirical formulations, Prec. Eng. 32 (2) (2008) 63–70.

[23] V. Lee, J. Gibert, J. Ziegert, Hybrid bi-directional flexure joint, Precis. Eng. 38 (2) (2013) 270–278.

[24] A. Shooshtari, R. Khajavi, An efficient procedure to find shape functions and stiffness matrices of nonprismatic Euler–Bernoulli and Timoshenko beam elements, Eur. J. Mech. A Solids 29 (5) (2010) 826–836, http://dx.doi.org/10.1016/j.euromechsol.2010.04.003.

[25] G. Balduzzi, M. Aminbaghai, E. Sacco, J. Füssl, J. Eberhardsteiner, F. Auricchio, Non-prismatic beams: A simple and effective Timoshenko-like model, Int. J. Solids Struct. 90 (2016) 236–250, http://dx.doi.org/10.1016/j.ijsolstr.2016.02.017.

[26] N. Lobontiu, J.S. Paine, E. Garcia, M. Goldfarb, Design of symmetric conic-section flexure hinges based on closed-form compliance equations, Mech. Mach. Theory 37 (5) (2002) 477–498.

[27] R.C. Shi, W. Dong, Z.J. Du, Design methodology and performance analysis of application-oriented flexure hinges, Rev. Sci. Instrum. 84 (7) (2013) 075005, http://dx.doi.org/10.1063/1.4813252.

[28] N.-H. Nguyen, M.-Y. Lee, J.-S. Kim, D.-Y. Lee, Compliance matrix of a single-bent leaf flexure for a modal analysis, Shock Vib. 2015 (672831) (2015) 1–10, http://dx.doi.org/10.1155/2015/672831.

[29] M.B. Fuchs, The unit-load method, in: Structures and their Analysis, Springer International Publishing, 2016, pp. 85–110.

[30] Q. Li, C. Pan, X. Xu, Closed-form compliance equations for power-function-shaped flexure hinge based on unit-load method, Precis. Eng. 37 (1) (2013) 135–145, http://dx.doi.org/10.1016/j.precisioneng.2012.07.010.

[31] K.E. Bisshopp, D.C. Drucker, Large deflection of cantilever beams, Q. Appl. Math. 3 (3) (1945) 272–275.

[32] F.V. Rohde, Large deflection of cantilever beam with a uniformly distributed load, Quart. Appl. Math. 11 (1953) 337–338.

[33] H.D. Conway, The nonlinear bending of thin circular rods, J. Appl. Mech. 23 (1) (1956) 7–10.

[34] A.E. Seames, H.D. Conway, A numerical procedure for calculating the large deflections of straight and curved beams, J. Appl. Mech. 24 (1957) 289–294.

[35] A. Nallathambi, C. Lakshmana Rao, S. Srinivasan, Large deflection of constant curvature cantilever beam under follower load, Int. J. Mech. Sci. 52 (3) (2010) 440–445.

[36] K. Lee, Large deflections of cantilever beams of non-linear elastic material under a combined loading, Int. J. Non-Linear Mech. 37 (3) (2002) 439–443.

[37] L. Chen, An integral approach for large deflection cantilever beams, Int. J. Non-Linear Mech. 45 (3) (2010) 301–305.

[38] M. Simi, N. Tolou, P. Valdastri, J.L. Herder, A. Menciassi, P. Dario, Modeling of a compliant joint in a Magnetic Levitation System for an endoscopic camera, Mech. Sci. 3 (1) (2012) 5–14.

[39] A. Kimiaeifar, N. Tolou, A. Barari, J. Herder, Large deflection analysis of cantilever beam under end point and distributed loads, J. Chin. Inst. Eng. 37 (4) (2014) 438–445.

[40] A. Cammarata, G. Sequenzia, S.M. Oliveri, G. Fatuzzo, Modified chain algorithm to study planar compliant mechanisms, Int. J. Interact. Des. Manuf. (IJIDeM) 10 (2) (2016) 191–201, http://dx.doi.org/10.1007/s12008-016-0299-2.

[41] G. Chen, F. Ma, R. Bai, W. Zhu, S.P. Magleby, L.L. Howell, An energy-based framework for nonlinear kinetostatic modeling of compliant mechanisms utilizing beam flexures, J. Comput. Inf. Sci. Eng. 21 (6) (2021) 1–18, http://dx.doi.org/10.1115/1.4050472.

[42] A. Zhang, G. Chen, A comprehensive elliptic integral solution to the large deflection problems of thin beams in compliant mechanisms, J. Mech. Robotics 5 (2) (2013) 021006, http://dx.doi.org/10.1115/1.4023558.

[43] A. Cammarata, M. Lacagnina, G. Sequenzia, Alternative elliptic integral solution to the beam deflection equations for the design of compliant mechanisms, Int. J. Interact. Des. Manuf. (IJIDeM) 13 (2) (2018) 499–505, http://dx.doi.org/10.1007/s12008-018-0512-6.

[44] F. Ma, G. Chen, Modeling large planar deflections of flexible beams in compliant mechanisms using chained beam-constraint-model, J. Mech. Robotics 8 (2) (2016) 021018.

[45] G. Chen, F. Ma, G. Hao, W. Zhu, Modeling large deflections of initially curved beams in compliant mechanisms using chained beam constraint model, J. Mech. Robotics 11 (1) (2019) 011002.
[46] K. Wu, G. Zheng, G. Chen, S. Awtar, A body-frame beam constraint model, Mech. Mach. Theory 192 (2024) 105517, http://dx.doi.org/10.1016/j.mechmachtheory.2023.105517.
[47] L.L. Howell, A. Midha, A method for the design of compliant mechanisms with small-length flexural pivots, J. Mech. Robotics 116 (1) (1994) 280–290.
[48] L.L. Howell, A. Midha, Parametric deflection approximations for end-loaded, large-deflection beams in compliant mechanisms, J. Mech. Robotics 117 (1) (1995) 156–165.
[49] M.H. Dado, Variable parametric pseudo-rigid-body model for large-deflection beams with end loads, Int. J. Non-Linear Mech. 36 (7) (2001) 1123–1133.
[50] C. Kimball, L.-W. Tsai, Modeling of flexural beams subjected to arbitrary end loads, Trans. ASME, J. Mech. Des. 124 (2) (2002) 223–235.
[51] Y.-Q. Yu, P. Zhou, Q.-P. Xu, A new pseudo-rigid-body model of compliant mechanisms considering axial deflection of flexural beams, in: New Trends in Mechanism and Machine Science, Springer, 2015, pp. 851–858.
[52] H.-J. Su, A pseudorigid-body 3R model for determining large deflection of cantilever beams subject to tip loads, J. Mech. Robotics 1 (2) (2009) 021008.
[53] S. Šalinić, A. Nikolić, A new pseudo-rigid-body model approach for modeling the quasi-static response of planar flexure-hinge mechanisms, Mech. Mach. Theory 124 (2018) 150–161.
[54] S.-K. Zhu, Y.-Q. Yu, Pseudo-rigid-body model for the flexural beam with an inflection point in compliant mechanisms, J. Mech. Robotics 9 (3) (2017) 031005.
[55] Y.-Q. Yu, S.-K. Zhu, 5R pseudo-rigid-body model for inflection beams in compliant mechanisms, Mech. Mach. Theory 116 (2017) 501–512.
[56] M. Jin, X. Zhang, A new topology optimization method for planar compliant parallel mechanisms, Mech. Mach. Theory 95 (2016) 42–58, http://dx.doi.org/10.1016/j.mechmachtheory.2015.08.016.
[57] S. Koppen, M. Langelaar, F. van Keulen, A simple and versatile topology optimization formulation for flexure synthesis, Mech. Mach. Theory 172 (2022) 104743, http://dx.doi.org/10.1016/j.mechmachtheory.2022.104743.
[58] K. Liang, D. Zhu, J. Liu, Topology optimization of a spatial compliant parallel mechanism based on constant motion transmission characteristic matrix, Mech. Mach. Theory 180 (2023) 105125, http://dx.doi.org/10.1016/j.mechmachtheory.2022.105125.
[59] M. Verotti, Analysis of the center of rotation in primitive flexures: Uniform cantilever beams with constant curvature, Mech. Mach. Theory 97 (2016) 29–50.
[60] M. Verotti, Effect of initial curvature in uniform flexures on position accuracy, Mech. Mach. Theory 119 (2018) 106–118.
[61] M. Verotti, A pseudo-rigid body model based on finite displacements and strain energy, Mech. Mach. Theory 149 (2020) 103811.
[62] P.P. Valentini, E. Pennestrì, Second-order approximation pseudo-rigid model of leaf flexure hinge, Mech. Mach. Theory 116 (2017) 352–359.
[63] P.P. Valentini, M. Cirelli, E. Pennestrì, Second-order approximation pseudo-rigid model of flexure hinge with parabolic variable thickness, Mech. Mach. Theory 136 (2019) 178–189, http://dx.doi.org/10.1016/j.mechmachtheory.2019.03.006.
[64] M. Cera, M. Cirelli, L. Colaiacovo, P.P. Valentini, Second-order approximation pseudo-rigid model of circular arc flexure hinge, Mech. Mach. Theory 175 (2022) 104963, http://dx.doi.org/10.1016/j.mechmachtheory.2022.104963.
[65] M. Krause, Analysis der ebenen Bewegung, Walter de Gruyter GmbH & Co KG, 2021.
[66] G.R. Veldkamp, Canonical systems and instantaneous invariants in spatial kinematics, J. Mech. 2 (3) (1967) 329–388, http://dx.doi.org/10.1016/0022-2569(67)90006-7.
[67] O. Bottema, B. Roth, Theoretical Kinematics, vol. 24, Courier Corporation, 1990.
[68] A. Inalcik, S. Ersoy, H. Stachel, On instantaneous invariants of hyperbolic planes, Math. Mech. Solids 22 (5) (2015) 1047–1057, http://dx.doi.org/10.1177/1081286515616283.